

Structural and dynamical properties of the percolation backbone in two and three dimensions

Markus Porto,¹ Armin Bunde,^{1,2} Shlomo Havlin,^{1,2} and H. Eduardo Roman¹

¹*Institut für Theoretische Physik III, Justus-Liebig-Universität Giessen, Heinrich-Buff-Ring 16, 35392 Giessen, Germany*

²*Minerva Center and Department of Physics, Bar-Ilan University, 52900 Ramat-Gan, Israel*

(Received 1 October 1996)

We study structural and dynamical properties of the backbone of the incipient infinite cluster for site percolation in two and three dimensions. We calculate the average mass of the backbone in chemical ℓ space, $\langle M_B(\ell) \rangle \sim \ell^{d_\ell^B}$, where d_ℓ^B is the chemical dimension. We find $d_\ell^B = 1.45 \pm 0.01$ in $d=2$ and $d_\ell^B = 1.36 \pm 0.02$ in $d=3$. The fractal dimension in r space d_f^B is obtained from the relation $d_f^B = d_\ell^B d_{\min}^B$, $d_f^B = 1.64 \pm 0.02$ in $d=2$ and $d_f^B = 1.87 \pm 0.03$ in $d=3$, where d_{\min}^B is the fractal dimension of the shortest path. The distribution function $\Phi_B(r, \ell)$ is determined, giving the probability of finding two backbone sites at the spatial distance r connected by the shortest path of length ℓ , as well as the related quantity $\ell_{\min}^B(r, N_{\text{av}})$, giving the length of the minimal shortest path for two backbone sites at distance r as a function of the number N_{av} of configurations considered. Regarding dynamical properties, we study the distribution functions $P_B(\ell, t)$ and $P_B(r, t)$ of random walks on the backbone, giving the probability of finding a random walker after t time steps, at a chemical distance ℓ , and Euclidean distance r from its starting point, respectively, and their first moments $\langle \ell_B(t) \rangle \sim t^{1/d_w^B}$ and $\langle r_B(t) \rangle \sim t^{1/d_w^B}$, from which the fractal dimensions of the random walk d_w^{ℓ} and d_w^B are estimated. We find $d_w^{\ell} = 2.28 \pm 0.03$ and $d_w^B = 2.62 \pm 0.03$ in $d=2$ as well as $d_w^{\ell} = 2.25 \pm 0.03$ and $d_w^B = 3.09 \pm 0.03$ in $d=3$. [S1063-651X(97)00508-4]

PACS number(s): 05.20.-y, 05.40.+j, 64.60.-i, 66.30.-h

I. INTRODUCTION

Percolation represents a useful model for a variety of systems in many fields of science displaying both structural disorder and self-similarity, i.e., fractal behavior, within some range of length scales [1–3]. In many circumstances, a detailed knowledge of the internal structure of percolation clusters is required. In particular, for studying transport processes near the percolation threshold p_c , a crucial role is played by the complex topology of the available conducting paths [4–7].

It is known that at p_c , the incipient infinite cluster exhibits a variety of self-similar substructures and consequently a rich scenario of transport properties [4–7]. A prominent role is played by the backbone of the cluster, defined as the subset of cluster sites carrying the current when a voltage difference is applied between two sites (see [8] and references therein). Thus, the backbone structure solely determines the conductivity of the whole percolation network between both sites. The backbone of a percolation cluster is also useful as a model of a porous medium containing long polymer chains [9]. So far, much is known about structural and dynamical properties of percolation clusters, but little is known about the corresponding properties of the backbone.

In this paper, we report a detailed study of structural and dynamical properties of the backbone of the incipient infinite cluster at p_c in two and three dimensions. Actually, many of the exponents characterizing the structural and dynamical properties of the backbone are presently poorly known, in particular, in three dimensions. To obtain accurate results, we study the backbone in topological or chemical space [3,5]. The topological or chemical distance ℓ between two points on the cluster is defined as the length of the shortest path connecting them via nearest-neighbor cluster sites.

Since our clusters are generated in chemical space (see below), this is the natural metric for measuring critical exponents. To this end, we first calculate the fractal dimension of the backbone in chemical space (ℓ space) d_ℓ^B , and obtain the fractal dimension in Euclidean space (r space) d_f^B , from the relation $d_f^B = d_\ell^B d_{\min}^B$, where d_{\min}^B is the fractal dimension of the shortest path [3,5]. We next study the distribution function $\Phi_B(r, \ell)$, giving the probability that two backbone sites at distance r from each other are connected by a shortest path of length ℓ , as well as the related quantity $\ell_{\min}^B(r, N_{\text{av}})$, giving the length of the minimal shortest path for backbone sites at distance r from each other as a function of the number N_{av} of configurations considered. To the best of our knowledge, these quantities have not been studied so far for the backbone. It is therefore interesting to calculate $\Phi_B(r, \ell)$ and compare it with the corresponding structural function $\Phi(r, \ell)$ for the whole cluster, which is now known quite accurately (for a recent work see Ref. [10]). From the additional information obtained by studying $\Phi_B(r, \ell)$, we expect to better understand the structural properties of the whole cluster as well.

Regarding dynamical properties, we consider random walks on the backbone and calculate the mean square displacements of the walker as a function of time, in both ℓ and r spaces. Finally, we consider the corresponding distribution functions $P_B(\ell, t)$ and $P_B(r, t)$, giving the probability density that the walker is, at time t , at the distance ℓ and r , respectively, from its starting point at $t=0$. Following the study of $P(r, t)$ for the whole cluster [11], we also discuss the question of the dependence of $P_B(r, t)$ on the number N_{av} of backbone configurations taken into account in the average.

The paper is organized as follows. In Sec. II, the fractal dimensions in chemical and Euclidean space are determined,

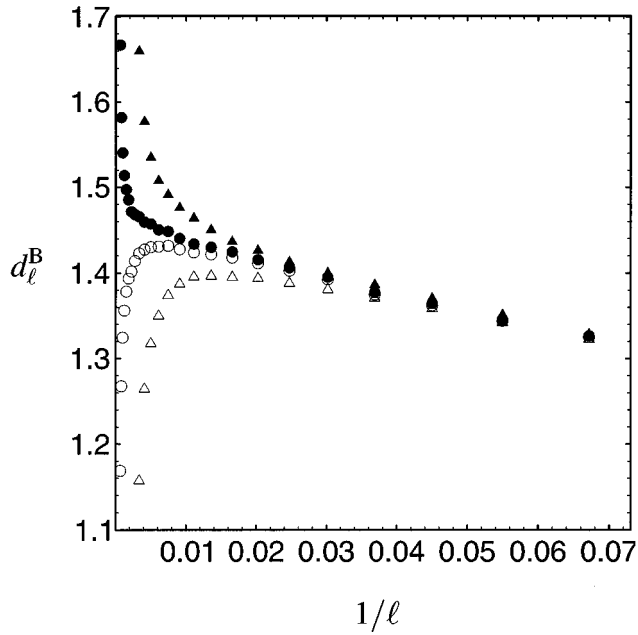


FIG. 1. Plot of the chemical dimension d_ℓ^B as a function of $1/\ell$ for $d=2$ [obtained from successive slopes of $\ln M_B(\ell)$ vs $\ln \ell$]. The backbone is determined using *one* site on the last grown chemical shell (open symbols) and *all* sites on the last grown chemical shell (full symbols). The plots are based on averages of $M_B(\ell)$ over 80 000 cluster configurations, with a maximum chemical distance $\ell_{\max}=2000$ (open and full circles) and $\ell_{\max}=400$ (open and full triangles). The results are summarized in Table I.

together with the distribution function of the Euclidean distance r between two backbone sites as a function of their chemical distance ℓ , and the scaling behavior of the shortest path. In Sec. III, we study random walks on the backbone, both in chemical and Euclidean space, and determine the corresponding distribution functions as well as their first moments. Finally, in Sec. IV, we summarize our results.

II. STRUCTURAL PROPERTIES

We generate large percolation clusters at criticality with the well-known Leath algorithm [12] on square and simple cubic lattices. The Leath algorithm generates in every step t the whole set of sites having a chemical distance $\ell=t$ from the seed, i.e., in the first step all sites with $\ell=1$ are generated, in the second step all sites with $\ell=2$ and so on. The corresponding backbone is obtained using an improved version of the ‘‘burning’’ algorithm [8] described in detail in Appendix A. To perform the averages, we grow clusters up to a maximum chemical distance ℓ_{\max} from the seed, with $\ell_{\max}=2000$ in two dimensions and $\ell_{\max}=1000$ in three dimensions. To minimize the computer memory needed for the calculations, we estimate the minimum lattice sizes L required to generate such large clusters from a relation given in [11] (see Appendix B for details). We use $L=2801$ in $d=2$ and $L=685$ in $d=3$, which in both cases are much smaller than $L'=2\ell_{\max}+1$. Nevertheless, *none* of the generated clusters reached the lattice boundaries. This more efficient use of computer memory, as well as the improved burning algorithm, enables us to study much larger systems than before, leading to more accurate estimates for the criti-

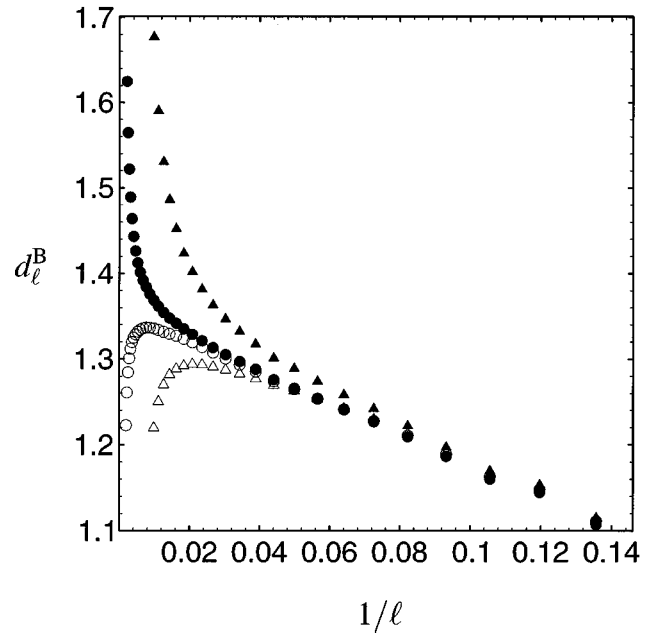


FIG. 2. Plot of the chemical dimension d_ℓ^B as a function of $1/\ell$ for $d=3$ [obtained from successive slopes of $\ln M_B(\ell)$ vs $\ln \ell$]. The backbone is determined using *one* site on the last grown chemical shell (open symbols) and *all* sites on the last grown chemical shell (full symbols). The plots are based on averages of $M_B(\ell)$ over 80 000 cluster configurations, with a maximum chemical distance $\ell_{\max}=1000$ (open and full circles) and $\ell_{\max}=200$ (open and full triangles). The results are summarized in Table I.

cal exponents and the fractal dimensions.

A. Fractal dimensions

Because the clusters are generated in chemical space, no boundary effects occur when looking at properties that depend on the chemical distance ℓ , in contrast to Euclidean space (r space), where strong boundary effects are present. Thus, the fractal dimension d_f^B of the backbone, defined by $\langle M_B(r) \rangle \sim r^{d_f^B}$, is not determined directly, but instead we study the mass-distance relation in ℓ space according to

$$\langle M_B(\ell) \rangle \sim \ell^{d_\ell^B}, \quad (1)$$

where d_ℓ^B is the fractal dimension of the backbone in chemical space. The two fractal dimensions are related by $d_f^B = d_\ell^B d_{\min}^B$, where d_{\min}^B is the fractal dimension of the shortest path and describes the scaling between r and ℓ , i.e., $\langle \ell(r) \rangle \sim r^{d_{\min}^B}$, with $d_{\min}^B = 1.130 \pm 0.004$ in $d=2$ [13,14] and $d_{\min}^B = 1.374 \pm 0.004$ in $d=3$ [15].

The results for d_ℓ^B are displayed in Fig. 1 for $d=2$, and in Fig. 2 for $d=3$, where the successive slopes of $\ln M_B(\ell)$ vs $\ln \ell$ as a function of $1/\ell$ are shown. The open symbols correspond to the case in which the backbone is defined between the seed and *one* randomly chosen site on the last grown chemical shell. Clearly, in this case the value of d_ℓ^B tends to decrease when $\ell \rightarrow \ell_{\max}$, since close to ℓ_{\max} the backbone grows nearly linear. This provides us with a numerical lower bound for the actual value of d_ℓ^B . A numerical upper bound can be obtained by defining the backbone between the seed and *all* sites on the last grown chemical shell.

TABLE I. The chemical dimension d_{ℓ}^B of the backbone obtained from Figs. 1 and 2. The fractal dimensions d_f^B are calculated from the relation $d_f^B = d_{\ell}^B d_{\min}^B$, with $d_{\min}^B = 1.130 \pm 0.004$ ($d=2$) [13,14] and $d_{\min}^B = 1.374 \pm 0.004$ ($d=3$) [15].

| Fractal dimension | Lattice dimension | | |
|-------------------|-------------------|-----------------|------------|
| | $d=2$ | $d=3$ | $d \geq 6$ |
| d_{ℓ}^B | 1.45 ± 0.01 | 1.36 ± 0.02 | 1 |
| d_f^B | 1.64 ± 0.02 | 1.87 ± 0.03 | 2 |

The full symbols correspond to this case, where now the value of d_{ℓ}^B tends to increase when $\ell \rightarrow \ell_{\max}$, since close to ℓ_{\max} the so defined backbone coincides with the cluster itself. Our estimated asymptotic values, obtained by fitting two straight lines for both the lower and upper sets of points, and extrapolating $1/\ell \rightarrow 0$, are reported in Table I. The reported exponents d_{ℓ}^B are the averages of these extrapolations, while the extrapolated values allow us to estimate the error bars. The obtained values are consistent with previously published results, see, e.g., [8].

B. Distribution functions

Next, we consider the structural distribution function $\Phi_B(r, \ell)$, giving the probability that two backbone sites connected by a shortest path of length ℓ are at spatial distance r from each other. We assume for $\Phi_B(r, \ell)$ a similar scaling form as for the entire cluster (see e.g., [5,10,14]), i.e.,

$$\Phi_B(r, \ell) = \frac{1}{r^{\tilde{\nu}d}} f_B(x), \quad (2)$$

with the scaling variable $x = r/\ell^{\tilde{\nu}}$ and $\tilde{\nu} \equiv 1/d_{\min}^B$, and $\Phi_B(r, \ell) = 0$ for $\ell < \ell_{\min}^B(r, N_{\text{av}})$. The quantity $\ell_{\min}^B(r, N_{\text{av}})$ is discussed in detail in Sec. III. As for the entire cluster [10], we expect that the scaling function $f_B(x)$ cannot be fitted by a simple product of a power law and an exponential function, but displays a more general form

$$f_B(x) = \begin{cases} c_1^B x^{g_1^B} & \text{for } x \ll 1, \\ c_2^B x^{g_2^B} \exp[-a_B x^{\delta}] & \text{for } x \gg 1, \end{cases} \quad (3)$$

with two different exponents g_1^B and g_2^B in the regimes $r/\ell^{\tilde{\nu}} \ll 1$ and $r/\ell^{\tilde{\nu}} \gg 1$, respectively, and $\delta \equiv (1 - \tilde{\nu})^{-1}$. The normalization is given in the embedding d -dimensional space by $\int r^{d-1} \Phi_B(r, \ell) dr = 1$. For convenience, we determine numerically the distribution function $\tilde{\Phi}_B(r, \ell)$, related to $\Phi_B(r, \ell)$ by

$$\tilde{\Phi}_B(r, \ell) = r^{d-1} \Phi_B(r, \ell) = \frac{1}{r} \left(\frac{r}{\ell^{\tilde{\nu}}} \right)^d f_B(x), \quad (4)$$

which is normalized according to $\int \tilde{\Phi}_B(r, \ell) dr = 1$. The function $r \tilde{\Phi}_B(r, \ell)$ vs $r/\ell^{\tilde{\nu}}$ is shown in Fig. 3 for $d=2$ and

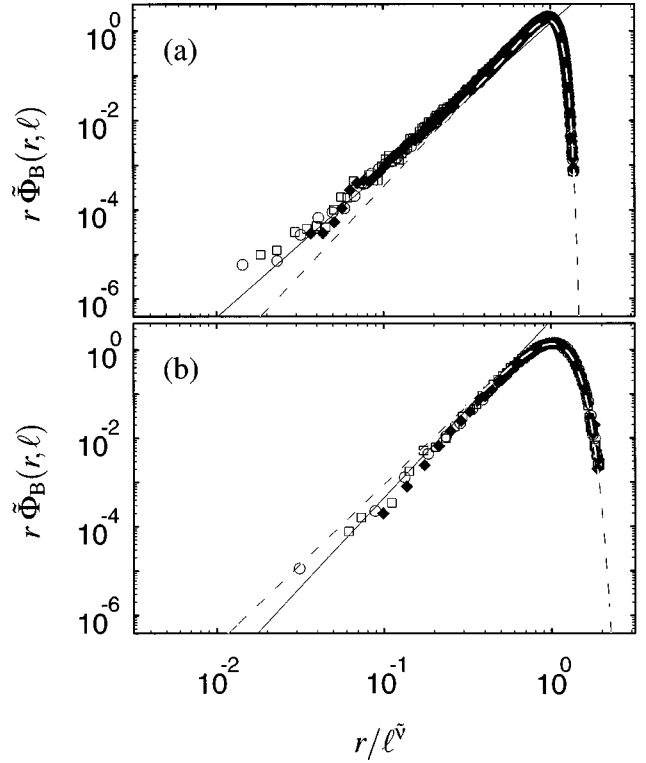


FIG. 3. Scaling plots of the distribution function for percolation backbones $r \tilde{\Phi}_B(r, \ell)$ vs $r/\ell^{\tilde{\nu}}$, for (a) $d=2$, $\ell=1000$ (circle), $\ell=1400$ (full diamond), and $\ell=1800$ (square), and (b) $d=3$, $\ell=400$ (circle), $\ell=600$ (full diamond), and $\ell=800$ (square). In both cases, the plots are based on averages over 80 000 cluster configurations, with a maximum chemical distance $\ell_{\max} = 2000$ in $d=2$ and $\ell_{\max} = 1000$ in $d=3$. The lines represent our fits for $r/\ell^{\tilde{\nu}} \ll 1$ (continuous line) and $r/\ell^{\tilde{\nu}} \gg 1$ (dashed line). The fitting parameters are summarized in Table II.

$d=3$, from which the exponents \tilde{g}_1^B and \tilde{g}_2^B are determined, which are related to g_1^B and g_2^B by $\tilde{g}_1^B = g_1^B + d$ and $\tilde{g}_2^B = g_2^B + d$, respectively. The results for the fitting parameters are reported in Table II. We note that the corresponding distribution function $\Phi_B^{(\text{all})}(r, \ell)$ for the backbone defined

TABLE II. The fitting parameters describing the scaling function $f_B(x)$ (see Fig. 3) for the backbone of percolation clusters at criticality, where $f_B(x) = c_1^B x^{g_1^B}$ for $x \ll 1$ (continuous line) and $f_B(x) = c_2^B x^{g_2^B} \exp[-a_B x^{\delta}]$ for $x \gg 1$ (dashed line), with $\delta \equiv (1 - \tilde{\nu})^{-1}$. The measured exponents \tilde{g}_1^B and \tilde{g}_2^B are related to g_1^B and g_2^B by $\tilde{g}_1^B = g_1^B + d$ and $\tilde{g}_2^B = g_2^B + d$.

| Structural exponents and prefactors | Lattice dimension | | |
|-------------------------------------|-------------------|-----------------|------------|
| | $d=2$ | $d=3$ | $d \geq 6$ |
| g_1^B | 1.30 ± 0.20 | 1.02 ± 0.20 | 0 |
| g_2^B | 1.97 ± 0.20 | 0.59 ± 0.20 | 0 |
| \tilde{g}_1^B | 3.30 ± 0.20 | 4.02 ± 0.20 | |
| \tilde{g}_2^B | 3.97 ± 0.20 | 3.59 ± 0.20 | |
| c_1^B | 1.50 ± 0.20 | 4.63 ± 0.20 | |
| c_2^B | 3.10 ± 0.20 | 3.43 ± 0.20 | |
| a_B | 0.62 ± 0.20 | 0.94 ± 0.20 | |

between the seed and all sites on the last grown chemical shell is identical to $\Phi_B(r, \ell)$ within the current numerical accuracy.

C. Minimal shortest path

We discuss next the behavior of the minimal shortest path $\ell_{\min}^B(r, N_{\text{av}})$ determining the values of ℓ at which $\Phi_B(r, \ell) = 0$. This quantity plays a very important role for determining transport properties: The fact that the minimal shortest path $\ell_{\min}^B(r, N_{\text{av}})$ shows an explicit dependence on the number of configurations N_{av} considered has important consequences for dynamical properties as, e.g., random walks, fractons or electronic wave functions [11]. In this paper we restrict ourselves to the discussion of the effect on random walks, see Sec. III.

We expect a scaling behavior of $\ell_{\min}^B(r, N_{\text{av}})$, as a function of the Euclidean distance r and the number of configurations N_{av} considered, similar to that on the entire cluster [11], i.e.,

$$\ell_{\min}^B(r, N_{\text{av}}) = \begin{cases} r & \text{for } r < r_c^B(N_{\text{av}}), \\ \alpha_{\min}^B(N_{\text{av}}) r^{d_{\min}} & \text{for } r > r_c^B(N_{\text{av}}). \end{cases} \quad (5)$$

Notice that below the crossover distance $r_c^B(N_{\text{av}})$, the minimal chemical distance $\ell_{\min}^B(r, N_{\text{av}})$ is independent of the number of configurations N_{av} considered, while for $r > r_c^B(N_{\text{av}})$ it depends explicitly on N_{av} . To obtain the crossover distance $r_c^B(N_{\text{av}})$ analytically, we consider the probability $W_{N_{\text{av}}}^B$ to find a shortest path of length $\ell = r = r_c^B$ within N_{av} backbone configurations, where $W_{N_{\text{av}}}^B = N_{\text{av}}^{-1}$ holds. For the entire cluster the relation $W_{N_{\text{av}}} = z p_c^{r_c}$ was used in [11], where z is the coordination number of the lattice. For the backbone we expect a similar relation $W_{N_{\text{av}}}^B = z_{\text{eff}} p_c^{r_c}$, where z is replaced by an effective coordination number z_{eff} , which incorporates the probability that the considered site belongs to the backbone. Since the backbone is more dilute than the whole cluster, we have in average a smaller connectivity, i.e., $z_{\text{eff}} < z$. This yields

$$r_c^B(N_{\text{av}}) = \frac{\ln z_{\text{eff}} + \ln N_{\text{av}}}{\ln(1/p_c)}, \quad (6)$$

where z_{eff} is not known analytically and must be determined *a posteriori*.

To determine $\alpha_{\min}^B(N_{\text{av}})$, we assume, as for the entire cluster, the scaling behavior $\ell_{\min}^B(r, N_{\text{av}}) = r_c^B(N_{\text{av}}) g_B[r/r_c^B(N_{\text{av}})]$. To fulfill Eq. (5), the scaling function $g_B(x)$ must behave as $g_B(x) = x$ when $x < 1$ and $g_B(x) \sim x^{d_{\min}}$ when $x > 1$. This yields

$$\alpha_{\min}^B(N_{\text{av}}) = \alpha_B [r_c^B(N_{\text{av}})]^{1-d_{\min}}, \quad (7)$$

where the prefactor α_B remains to be determined. Results for $\ell_{\min}^B(r, N_{\text{av}})/r_c^B(N_{\text{av}})$ versus $r/r_c^B(N_{\text{av}})$ for different values of N_{av} are shown in Fig. 4 for $d=2$ and $d=3$. The shown lines indicate the predicted exponents, 1 for $r/r_c^B(N_{\text{av}}) < 1$ and d_{\min} for $r/r_c^B(N_{\text{av}}) > 1$. The values of z_{eff} are determined such that the best data collapse is achieved, and $\alpha_B = x_{\times}^{1-d_{\min}}$,

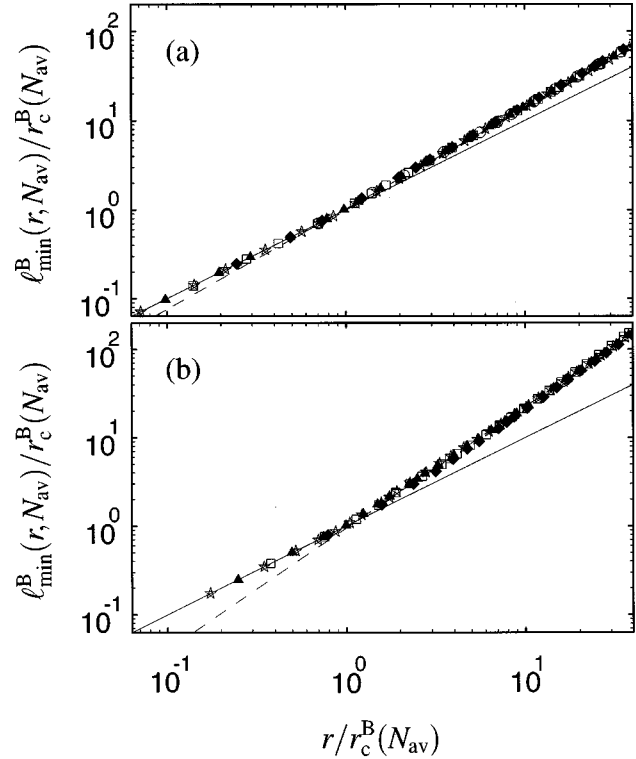


FIG. 4. Scaling plots of the minimum chemical distance $\ell_{\min}^B(r, N_{\text{av}})/r_c^B(N_{\text{av}})$ vs $r/r_c^B(N_{\text{av}})$, for (a) $d=2$ and (b) $d=3$, both for $N_{\text{av}}=1$ (circle), $N_{\text{av}}=4$ (full diamond), $N_{\text{av}}=20$ (square), $N_{\text{av}}=100$ (full triangle), and $N_{\text{av}}=750$ (star). In both cases, the plots are based on a total ensemble of 80 000 cluster configurations, with a maximum chemical distance $\ell_{\max}=2000$ in $d=2$ and $\ell_{\max}=1000$ in $d=3$. The lines represent the predicted exponent 1 for $r/r_c^B(N_{\text{av}}) < 1$ (continuous line) and d_{\min} for $r/r_c^B(N_{\text{av}}) > 1$ (dashed line). The results are summarized in Table III.

where x_{\times} is the value of $x = r/r_c^B(N_{\text{av}})$ at the crossover. The results are reported in Table III. We note that the corresponding structural quantity $\ell_{\min}^B(\text{all})(r, N_{\text{av}})$ for the backbone defined between the seed and all sites on the last grown chemical shell is identical to $\ell_{\min}^B(r, N_{\text{av}})$ within the current numerical accuracy.

III. DYNAMICAL PROPERTIES

In the following, we consider dynamical properties of the backbone by studying random walks, both in Euclidean and chemical space. To this end, we employ the exact enumeration method [5]. For the present purposes, clusters are grown on square and simple cubic lattices up to a maximum chemical distance $\ell_{\max}=1000$ in $d=2$ and $\ell_{\max}=400$ in $d=3$. Clusters which have not reached the chemical shell ℓ_{\max} are

TABLE III. Structural constants, defined in Eqs. (6) and (7) and obtained from the data collapse shown in Fig. 4.

| Structural constant | Lattice dimension | | |
|---------------------|-------------------|-----------------|------------|
| | $d=2$ | $d=3$ | $d \geq 6$ |
| z_{eff} | 2.1 ± 0.2 | 1.2 ± 0.2 | 1 |
| α_B | 1.02 ± 0.05 | 0.95 ± 0.07 | |

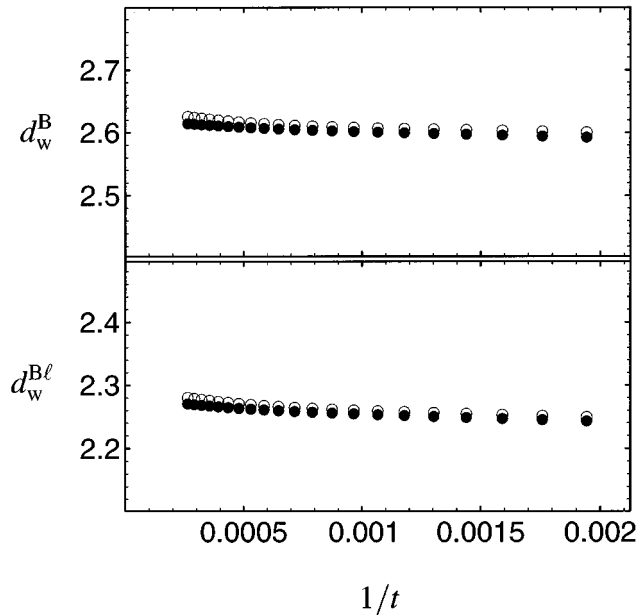


FIG. 5. Plot of the fractal dimensions d_w^B and $d_w^{B\ell}$ of the random walk as a function of $1/t$ for $d=2$ [obtained from successive slopes of $\ln r_B(t)$ and $\ln \ell_B(t)$ vs $\ln t$, respectively]. The backbone is determined using *one* site on the chemical shell ℓ_{\max} (open circles) and *all* sites on the chemical shell ℓ_{\max} (full circles). The plots are based on averages of $r_B(t)$ and $\ell_B(t)$ over 10 000 cluster configurations, with a maximum chemical distance $\ell_{\max}=1000$ and $t_{\max}=4000$ time steps. The results are summarized in Table IV.

discarded. Again, the lattice sizes are estimated with the method discussed in Appendix B. In our simulations, we consider random walks of $t_{\max}=4000$ and $t_{\max}=1600$ time steps in $d=2$ and $d=3$, respectively.

A. Mean displacements

The mean displacements after t time steps in chemical and Euclidean metric are given by

$$\langle \ell_B(t) \rangle \sim t^{1/d_w^{B\ell}} \quad (8)$$

and

$$\langle r_B(t) \rangle \sim t^{1/d_w^B}, \quad (9)$$

from which the fractal dimensions of the random walk $d_w^{B\ell}$ and d_w^B are determined. The results for $d_w^{B\ell}$ and d_w^B are displayed in Fig. 5 for $d=2$ and Fig. 6 for $d=3$, where the successive slopes of $\ln \ell_B(t)$ and $\ln r_B(t)$ vs $\ln t$ as a function of $1/t$ are shown. The open circles correspond to the case in which the backbone is defined between the seed and *one* randomly chosen site on the chemical shell ℓ_{\max} , and the full circles to the case in which the backbone is defined between the seed and *all* sites on the chemical shell ℓ_{\max} . Both sets of points coincide as long as the random walker mainly explores regions of the backbone where both algorithms yield similar structures. This provides us with numerical upper and lower bounds for the actual values of $d_w^{B\ell}$ and d_w^B . Our estimated asymptotic values, obtained by fitting two straight lines for both the lower and upper sets of points, and

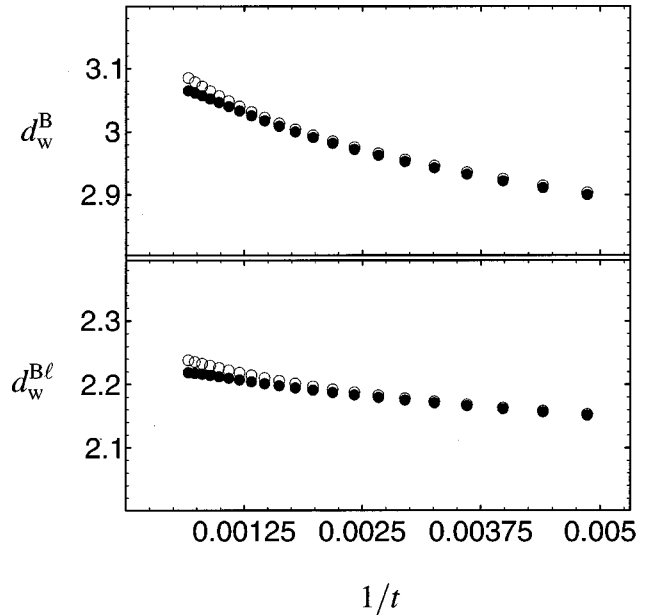


FIG. 6. Plot of the fractal dimensions d_w^B and $d_w^{B\ell}$ of the random walk as a function of $1/t$ for $d=3$ [obtained from successive slopes of $\ln r_B(t)$ and $\ln \ell_B(t)$ vs $\ln t$, respectively]. The backbone is determined using *one* site on the chemical shell ℓ_{\max} (open circles) and *all* sites on the chemical shell ℓ_{\max} (full circles). The plots are based on averages of $r_B(t)$ and $\ell_B(t)$ over 12 000 cluster configurations, with a maximum chemical distance $\ell_{\max}=400$ and $t_{\max}=1600$ time steps. The results are summarized in Table IV.

extrapolating $1/t \rightarrow 0$, are reported in Table IV. The reported exponents $d_w^{B\ell}$ and d_w^B are the averages of these extrapolations, while the extrapolated values allow us to estimate the error bars. The obtained values are consistent with previously published results, see, e.g., [16].

B. Distribution functions

The probability of a random walker to be at chemical distance ℓ and Euclidean distance r after t time steps is given by the distribution functions $P_B(\ell, t)$ and $P_B(r, t)$, respectively. The mean displacement $\langle \ell_B(t) \rangle$ and $\langle r_B(t) \rangle$ discussed above are the first moments of these distributions. For the distribution function in chemical space we expect a form similar to that for the entire cluster [5,6], i.e.,

$$\frac{P_B(\ell, t)}{P_B(0, t)} \sim \exp \left[- \left(\frac{\ell}{\xi_B} \right)^{v_B} \right], \quad (10)$$

TABLE IV. Summary of the results for the fractal dimensions $d_w^{B\ell}$ and d_w^B of the random walk on the backbone (see Figs. 5 and 6).

| Diffusion exponent | Lattice dimension | | |
|--------------------|-------------------|-----------------|------------|
| | $d=2$ | $d=3$ | $d \geq 6$ |
| $d_w^{B\ell}$ | 2.28 ± 0.03 | 2.25 ± 0.03 | 2 |
| d_w^B | 2.62 ± 0.03 | 3.09 ± 0.03 | 4 |

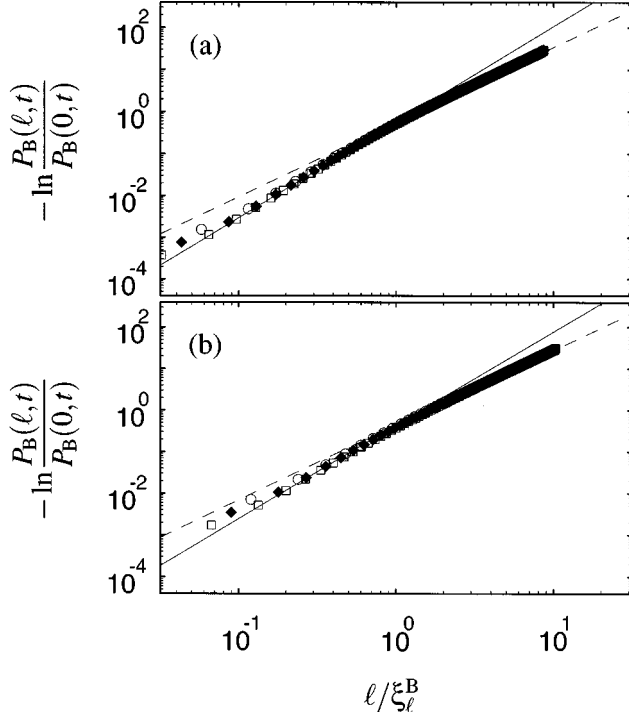


FIG. 7. Scaling plots of the distribution function $-\ln[P_B(\ell, t)/P_B(0, t)]$ vs ℓ/ξ_ℓ^B , for (a) $d=2$, $t=1000$ (circle), $t=2000$ (full diamond), and $t=4000$ (square), and (b) $d=3$, $t=400$ (circle), $t=800$ (full diamond), and $t=1600$ (square), with $\xi_\ell^B \sim \langle \ell_B(t) \rangle$. In both cases, the plots are based on averages over more than 10 000 cluster configurations, with a maximum chemical distance $\ell_{\max}=1000$ in $d=2$ and $\ell_{\max}=400$ in $d=3$. The lines represent the predicted exponents $d_w^{B'}$ for $\ell/\xi_\ell^B < 1$ (continuous line) and $d_w^{B'}/(d_w^{B'} - 1)$ for $\ell/\xi_\ell^B > 1$ (dashed line).

with $\xi_\ell^B \sim \langle \ell_B(t) \rangle$ and $P_B(0, t) \sim [\xi_\ell^B]^{-d^B}$, where $\langle \ell_B(t) \rangle$ is the mean displacement in chemical metric defined above. The distribution is normalized as $\int \ell^{d^B-1} P_B(\ell, t) d\ell = 1$. To obtain the exponent ν_B , we plot $-\ln[P_B(\ell, t)/P_B(0, t)]$ vs ℓ/ξ_ℓ^B in double logarithmic form in Fig. 7 for $d=2$ and $d=3$. Similar to the entire cluster, we find $\nu_B = d_w^{B'}$ for $\ell/\xi_\ell^B < 1$ and $\nu_B = d_w^{B'}/(d_w^{B'} - 1)$ for $\ell/\xi_\ell^B > 1$.

To analytically calculate the distribution function $P_B(r, t; N_{\text{av}}) \equiv \langle P_B(r, t) \rangle_{N_{\text{av}}}$ for a random walker in Euclidean space, averaged over N_{av} configurations, we follow Refs. [6,11] and write $P_B(r, t; N_{\text{av}})$ as a convolution integral of the distribution of a random walker in ℓ space, $P_B(\ell, t)$, and the structural function $\Phi_B(r, \ell)$, i.e.,

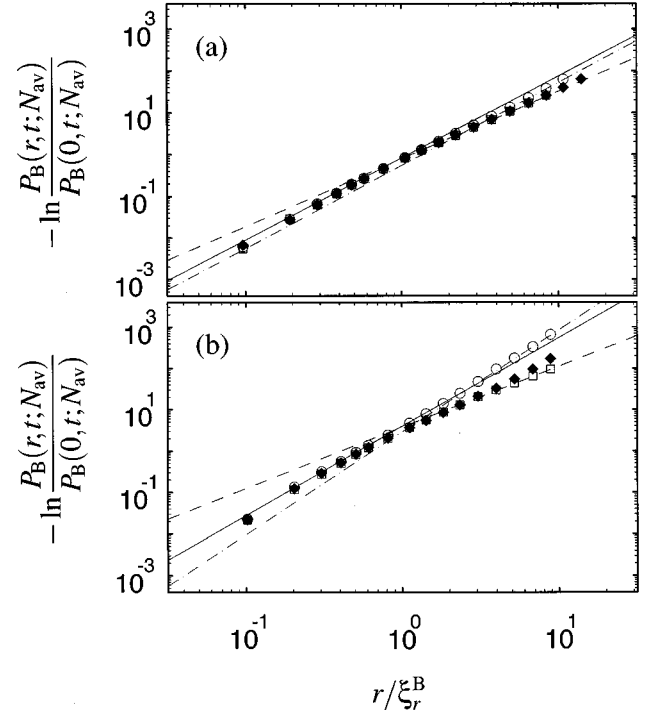


FIG. 8. Scaling plots of the distribution function $-\ln[P_B(r, t; N_{\text{av}})/P_B(0, t; N_{\text{av}})]$ vs r/ξ_r^B , for (a) $d=2$, $t=1000$ and (b) $d=3$, $t=400$, both for $N_{\text{av}}=1$, i.e., typical average (circle), $N_{\text{av}}=200$ (full diamond), and $N_{\text{av}}=10\,000$ (square), with $\xi_r^B \sim \langle r_B(t) \rangle$. In both cases, the plots are based on a total ensemble of more than 10 000 cluster configurations, with a maximum chemical distance $\ell_{\max}=1000$ and $\ell_{\max}=400$ in $d=2$ and $d=3$, respectively. The lines represent the predicted exponents $g_1^B + d - d_f^B$ for $r < r_1^B$ (continuous line), $d_w^{B'}/(d_w^{B'} - 1)$ for $r_1^B < r < r_\times(N_{\text{av}})$ (dashed line), and $d_w^{B'}/(d_w^{B'} - 1)$ for $r > r_\times(N_{\text{av}})$ (dashed-dotted line).

$$P_B(r, t; N_{\text{av}}) = r^{d-d_f^B} \int_{\ell_{\min}^B(r, N_{\text{av}})}^{\infty} \ell^{d^B-1} \Phi_B(r, \ell) P_B(\ell, t) d\ell, \quad (11)$$

where $\ell_{\min}^B(r, N_{\text{av}})$ is the length of the minimal shortest path discussed in Sec. II. The dependence of the lower integration limit $\ell_{\min}^B(r, N_{\text{av}})$ on the number of configurations N_{av} considered introduces a second crossover distance $r_\times(N_{\text{av}})$ and causes a dependence of $P_B(r, t; N_{\text{av}})$ on N_{av} . The distribution $P_B(r, t; N_{\text{av}})$ is normalized on the backbone by $\int r^{d_f^B-1} P_B(r, t; N_{\text{av}}) dr = 1$. Following the procedure described in [11,17], we obtain, in full analogy to the results for percolation clusters,

$$\frac{P_B(r, t; N_{\text{av}})}{P_B(0, t; N_{\text{av}})} \sim \begin{cases} 1 - c \left(\frac{r}{\xi_r^B} \right)^{g_1^B + d - d_f^B} & \text{for } r < r_1^B, \\ \exp \left[-c' \left(\frac{r}{\xi_r^B} \right)^{d_w^{B'}/(d_w^{B'} - 1)} \right] & \text{for } r_1^B < r < r_\times(N_{\text{av}}), \\ \exp \left[-c'' [r_c^B(N_{\text{av}})]^{d_w^{B'}/(d_{\min}^B - 1)/(d_w^{B'} - 1)} \left(\frac{r}{\xi_r^B} \right)^{d_w^{B'}/(d_w^{B'} - 1)} \right] & \text{for } r > r_\times(N_{\text{av}}) \end{cases} \quad (12)$$

(for the regime $r < r_1^B$ see also [18,19]). The crossover distances r_1^B and $r_\times^B(N_{av})$ are given by

$$r_1^B = \xi_r^B \left[\frac{(g_2^B + d)(d_{\min} - 1)}{a_B d_{\min}} \right]^{(d_w^B - 1)/d_w^B} \quad (13)$$

and

$$r_\times^B(N_{av}) = \xi_r^B \alpha_B^{-1/[d_w^B(d_{\min} - 1)/(d_w^B - 1)]} [r_c^B(N_{av})]^{(d_w^B - 1)/d_w^B}, \quad (14)$$

with $\xi_r^B \sim \langle r_B(t) \rangle$, where $\langle r_B(t) \rangle$ is the mean displacement in the Euclidean space defined above. Hence, for large distances r , the relevant length scale increases logarithmically with the number N_{av} of configurations. Below $r_\times^B(N_{av})$, $P_B(r, t) = P_B(r, t; N_{av})$ is independent of N_{av} , while above $r_\times^B(N_{av})$, the self-averaging hypothesis breaks down and $P_B(r, t; N_{av})$ depends logarithmically on N_{av} . The so-called typical average $\langle P_B(r, t) \rangle_{typ}$ is equivalent to the case $N_{av} = 1$, i.e., $\langle P_B(r, t) \rangle_{typ} \equiv P_B(r, t; 1)$.

To verify our predictions given in Eqs. (12)–(14), we plot $-\ln[P_B(r, t; N_{av})/P_B(0, t; N_{av})]$ vs r/ξ_r^B in double logarithmic form in Fig. 8 for $d=2$ and $d=3$. The shown lines indicate our predicted exponents $g_1^B + d - d_f^B$ for $r < r_1^B$, $d_w^B/(d_w^B - 1)$ for $r_1^B < r < r_\times^B(N_{av})$, and $d_w^B/(d_w^B - 1)$ for $r > r_\times^B(N_{av})$. The numerical data are well described by our analytical results.

IV. SUMMARY

In this paper we present extensive numerical simulations concerning the structural and dynamical properties of the backbone of percolation clusters at criticality in two and three dimensions. An improved burning algorithm, introduced in this work, enables us to study much larger systems than before, therefore leading to improved estimates for the fractal dimensions of the backbone d_ℓ^B and d_f^B , as well as for the corresponding fractal dimensions of the random walk d_w^B and d_w^B . We also calculate the structural distribution function $\Phi_B(r, \ell)$, the length of the minimal shortest path $\ell_{\min}^B(r, N_{av})$, and the distribution function of a random walker in chemical and Euclidean space $P_B(\ell, t)$ and $P_B(r, t; N_{av})$, respectively.

We note that from d_f^B and d_w^B the conductivity exponent $\tilde{\mu}$, which describes the scaling behavior of the conductivity σ of a percolation system near criticality as a function of the system size L , i.e., $\sigma \sim L^{-\tilde{\mu}}$, can be calculated by $\tilde{\mu} = d_w^B - d_f^B + d - 2$ [5,6]. Our results for d_f^B and d_w^B yield $\tilde{\mu} = 0.98 \pm 0.03$ in $d=2$ and $\tilde{\mu} = 2.22 \pm 0.03$ in $d=3$. These results are in very good agreement with the values $\tilde{\mu} = 0.97 \pm 0.01$ and $\tilde{\mu} = 2.2 \pm 0.1$ for $d=2$ and $d=3$, respectively, obtained from other simulations [3].

ACKNOWLEDGMENTS

We would like to thank M. Meyer, A. Ordemann, and S. Rabinovich for valuable discussions, as well as N. Conrad for his valuable assistance at the computer center of the Universität Giessen. This work has been supported by the Minerva Center for the Physics of Mesoscopics, Fractals and Neural Networks; the Alexander von Humboldt Foundation; and the Deutsche Forschungsgemeinschaft.

APPENDIX A: IMPROVED “BURNING” ALGORITHM

The backbones studied in this paper are generated using an improved version of the burning algorithm. The basic burning algorithm was first introduced in [8]. We review the above algorithm and consider its improvement.

To use the burning algorithm, one has to find the chemical distances ℓ to the starting site of the backbone and the sites where loops of cluster sites relative to the starting site close up (loop sites). Using the Leath method, the sites of the cluster are generated with increasing chemical distance ℓ from the seed. Therefore it is convenient to define the backbone between the seed (starting site) and one randomly chosen site on the last grown chemical shell of the cluster (end site) [20]. In such a case the chemical distances ℓ to the starting site are trivially identical to those obtained by Leath growth. By choosing the end site of the backbone on the last grown chemical shell we ensure that no sites with a larger chemical distance ℓ to the starting site than the end site exists. In addition, the loop sites are easy to identify during Leath growth, as they occur with increasing chemical distance ℓ from the seed.

The burning algorithm is divided into two parts. In the first part we start burning the end site, becoming a burning site. Then, its nearest-neighbor cluster sites are burnt, and become the new burning sites. This process is repeated from each burning site, with the condition that only nearest-neighbor sites are burnt which have a chemical distance ℓ to the starting site smaller than the burning site itself. This part of the burning algorithm ends when the starting site is reached. The thus obtained burnt sites are located along the shortest path between the starting and the end site, and form the so-called skeleton or elastic backbone [8,21]; an example is shown in Fig. 9(a).

In the second part of the algorithm we deal with the loop sites. At the beginning all loop sites are considered as active and stored in a list sorted by increasing chemical distance ℓ to the starting site. We start burning the first loop site, i.e., the one with the smallest chemical distance ℓ to the starting site, and proceed in the same way as for the skeleton. If during this process two or more different sites are reached which are known to be part of the backbone, then the burnt sites (including the loop site) belong to the backbone, and the corresponding loop site is no longer active and is removed from the list. Otherwise it cannot be decided yet whether these sites belong to the backbone or not, and one has to

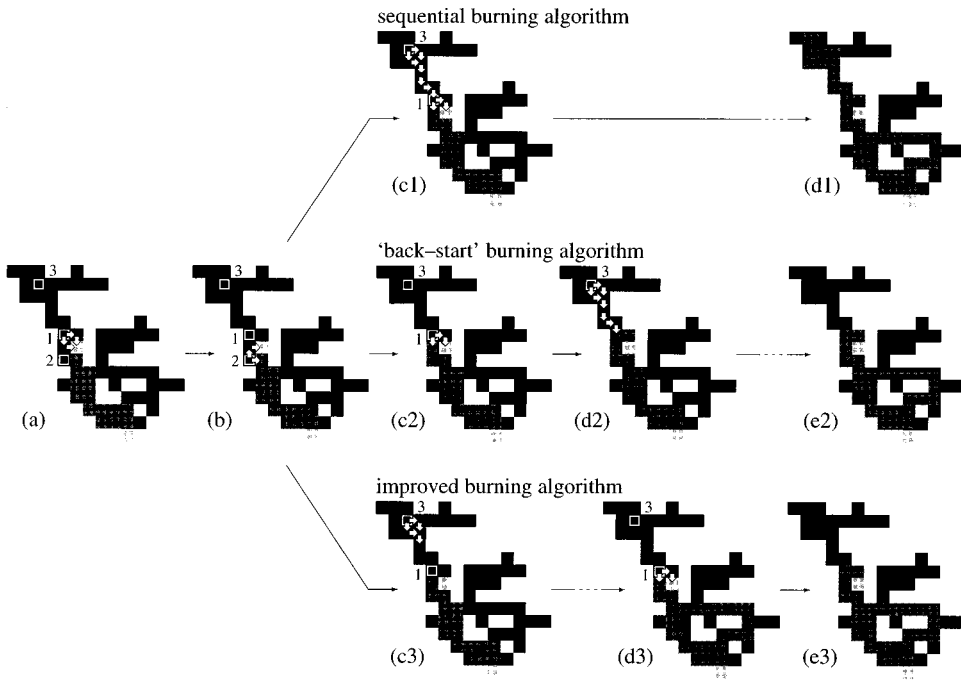


FIG. 9. Example for a configuration of a cluster and its backbone. The two end sites defining the backbone are colored in light gray, the sites found so far which belong to the backbone are in dark gray, and the remaining cluster in black. The cluster sites marked by a white square are loop sites, named “1,” “2,” and “3.” The white arrows indicate the burning processes and their directions, as discussed in Appendix A. The row at the top of the figure shows the different steps of the sequential burning algorithm with the erroneous result (d1), the row in the middle the “back-start” algorithm, and the row at the bottom the improved burning algorithm with the correct results (e2) and (e3), respectively.

restore the previous state of the burnt sites including the loop site, which remains active. In both cases one can continue treating the next loop site (having a chemical distance ℓ to the starting site equal or larger than the previous one) in the same way as described above. If the active loop site with the largest chemical distance ℓ has been considered, one starts from the active loop site with the smallest ℓ . The algorithm ends when no new site has been found belonging to the backbone during a complete run through the list of active loop sites.

However, this sequential algorithm described above generally produces erroneous results, such that sites not belonging to the backbone are added to it [see Fig. 9(c1) and (d1)]. To avoid such failures, one has to start again at the active loop site with the smallest chemical distance ℓ to the starting site whenever adding a new part to the backbone, instead of proceeding sequentially. By doing this, the backbone is determined correctly [see Fig. 9 (c2), (d2), and (e2)]. Unfortunately this “back-start” algorithm is very time consuming, since now the computing time depends quadratically on the number of loop sites [22].

The improvement of the algorithm is based on a simple observation: The reason for the erroneous outcome of the sequential version is due to the likely existence of so-called “tadpoles,” i.e., a group of sites which is linked to the actual backbone through a singly connected path. According to Fig. 9(a), the burning starting at the first loop site (denoted “1” in the figure) reaches the so far known backbone in one point, which coincides with the starting site. Therefore, the burnt sites are not identified as backbone sites and are restored to their previous state. A new burning process, starting from the next loop site, (denoted “2”), as shown in Fig. 9(b), reaches the backbone in two points, one is the starting site and the second a skeleton site (nearest-neighbor site of “2” to the right), and these burnt sites are correctly identified as backbone sites. Proceeding sequentially in the list of active loop sites in such a situation, i.e., by starting a burning process from the site “3,” as shown in Fig. 9 (c1), instead of

starting again at the active loop site with the smallest chemical distance ℓ to the starting site (i.e., site “1”), as shown in Fig. 9 (c2), yield the erroneous result shown in Fig. 9 (d1). This failure can be easily prevented, if it is realized during a burning process that only one site is burning during a burning step, reflecting the singly connected structure of the path, and the backbone has not yet been reached, see Fig. 9 (c3). In such a case, one can immediately stop the burning process from this loop site, keep the loop site active, and restore the previous state of the corresponding burnt sites. In addition, one can always proceed sequentially, even after adding a new part to the backbone, as shown in Fig. 9 (c3), (d3), and (e3), and as a result the computing time scales only linearly with the number of loop sites.

APPENDIX B: ESTIMATE FOR THE LATTICE SIZE FOR PERCOLATION CLUSTERS AT CRITICALITY

To minimize the computer memory needed for the simulations, we estimate the minimum lattice size $L = 2R + 1$ required to generate a cluster of ℓ_{\max} shells, with the condition that its radial extent r_{\max} will not exceed R . To this end, we employ the relation $\ell_{\min}(r, N_{\text{av}}) = \alpha_{\min}(N_{\text{av}}) r^{d_{\min}}$ [cf. Eq. (5)] valid in the regime $r > r_c(N_{\text{av}})$, where $\alpha_{\min}(N_{\text{av}}) = \alpha [r_c(N_{\text{av}})]^{1-d_{\min}}$, $\alpha \cong 1$, and $r_c(N_{\text{av}}) = (\ln z + \ln N_{\text{av}}) / \ln(1/p_c)$ [11]. From these relations one can estimate $r_{\max} \cong (\ell_{\max} / [\alpha_{\min}(N_{\text{av}})]^{1/d_{\min}})^{1/d_{\min}}$. In our simulations we consider typically $N_{\text{av}} \cong 10^6$ configurations, so that for determining, e.g., structural properties with $\ell_{\max} = 2000$ and $\ell_{\max} = 1000$ for $d = 2$ and $d = 3$, respectively, we estimate $r_{\max} \cong 1228$ and $r_{\max} \cong 309$. We have actually used $R = 1400$ and $R = 342$ in $d = 2$ and $d = 3$, respectively, which in both cases are much smaller than ℓ_{\max} , and actually correspond to the value of r_{\max} obtained with the above formula for more than 10^9 configurations.

- [1] *Fractals in Science*, edited by A. Bunde and S. Havlin (Springer, Berlin, 1994).
- [2] D. Stauffer and A. Aharony, *Introduction to Percolation Theory*, 2nd ed. (Taylor & Francis, London, 1992).
- [3] *Fractals and Disordered Systems*, edited by A. Bunde and S. Havlin, 2nd ed. (Springer, Berlin, 1996).
- [4] S. Alexander and R. Orbach, *J. Phys. (France) Lett.* **43**, L625 (1982).
- [5] S. Havlin and D. Ben-Avraham, *Adv. Phys.* **36**, 695 (1987).
- [6] A. Bunde, S. Havlin, and H.E. Roman, *Phys. Rev. A* **42**, 6274 (1990).
- [7] T. Nakayama, K. Yakubo, and R. Orbach, *Rev. Mod. Phys.* **66**, 381 (1994).
- [8] H.J. Herrmann, D.C. Hong, and H.E. Stanley, *J. Phys. A* **17**, L261 (1984).
- [9] H.E. Roman, J. Dräger, A. Bunde, S. Havlin, and D. Stauffer, *Phys. Rev. E* **52**, 6303 (1995).
- [10] H.E. Roman, *Phys. Rev. E* **51**, 5422 (1995).
- [11] A. Bunde and J. Dräger, *Physica A* **202**, 371 (1994); *Phys. Rev. E* **52**, 53 (1995).
- [12] P.L. Leath, *Phys. Rev. B* **14**, 5046 (1976); Z. Alexandrowicz, *Phys. Lett.* **80A**, 284 (1980).
- [13] H.J. Herrmann and H.E. Stanley, *J. Phys. A* **21**, L829 (1988).
- [14] A.U. Neumann and S. Havlin, *J. Stat. Phys.* **52**, 203 (1988).
- [15] P. Grassberger, *J. Phys. A* **25**, 5867 (1992).
- [16] H. Nakanishi, in *Annual Reviews of Computational Physics*, edited by D. Stauffer (World Scientific, Singapore, 1994).
- [17] J. Dräger, S. Russ, and A. Bunde, *Europhys. Lett.* **31**, 425 (1995).
- [18] S. Rabinovich, H.E. Roman, S. Havlin, and A. Bunde, *Phys. Rev. E* **54**, 3606 (1996).
- [19] H.E. Roman (unpublished).
- [20] Another possibility is to take all sites on the last grown chemical shell as end sites. In this case the method can be used in the same way as for a single end site, with the additional prescription that in the first part of the algorithm the burning starts simultaneously from all end sites.
- [21] S. Havlin, R. Nossal, B. Trus, and G.H. Weiss, *J. Phys. A* **17**, L957 (1984).
- [22] It has been shown that the number of loop sites N_{loop} scales as $N_{\text{loop}} \sim \ell^{d_f}$ [23]. If we start at the very beginning of the list whenever deleting a loop site out of it, the computing time is of the order $O(N_{\text{loop}}^2) = O(\ell^{2d_f})$. For the improved version the time is only of order $O(N_{\text{loop}}) = O(\ell^{d_f})$.
- [23] F. Tzschichholz, A. Bunde, and S. Havlin, *Phys. Rev. A* **39**, 5470 (1989).